materials

Article

Influence of Annealing Process on Soft Magnetic Properties of Fe-B-C-Si-P Amorphous Alloys

Jili Jia [1], You Wu [1], Lingxiang Shi [1,2], Ranbin Wang [1], Wenhui Guo [1], Hengtong Bu [1], Yang Shao [1], Na Chen [1] and Kefu Yao [1,*]

[1] School of Materials Science and Engineering, Tsinghua University, Beijing 100084, China
[2] Department of Mechanical Engineering, City University of Hong Kong, Tat Chee Avenue, Kowloon, Hong Kong
* Correspondence: kfyao@mail.tsinghua.edu.cn

Abstract: It is well known that the annealing process plays a key role in tuning the properties of Fe-based amorphous soft magnetic alloys. However, the optimal annealing process for a particular amorphous alloy is often difficult to determine. Here, $Fe_{81.4}B_{13.2}C_{2.8}Si_{1.8}P_{0.8}$ and $Fe_{82.2}B_{12.4}C_{2.8}Si_{1.8}P_{0.8}$ amorphous alloys (denoted as $Fe_{81.4}$ and $Fe_{82.2}$) were prepared to systematically study the effects of the annealing temperature and time on the soft magnetic properties. The results show that the optimum annealing temperature ranges of the $Fe_{81.4}$ and $Fe_{82.2}$ amorphous alloys were 623 K to 653 K and 593 K to 623 K, and their coercivity (H_c) values were only 2.0–2.5 A/m and 1.3–2.7 A/m, respectively. Furthermore, a characteristic temperature T_{ai} was obtained to guide the choosing of the annealing temperature at which the dB_s/dT begins to decrease rapidly. Based on the theory of spontaneous magnetization, the relationship between T_{ai} and the optimum annealing temperature ranges was analyzed. When the annealing temperature was higher than T_{ai}, the effect of the internal magnetic field generated by spontaneous magnetization on the relaxation behavior was significantly reduced, and the alloys exhibited excellent soft magnetic properties. It is worth indicating that when annealed at 603 K (slightly higher than T_{ai}), the $Fe_{82.2}$ amorphous alloys exhibited excellent and stable soft magnetic properties even if annealed for a long time. The H_c of $Fe_{82.2}B_{12.4}C_{2.8}Si_{1.8}P_{0.8}$ amorphous alloys was only 1.9 A/m when annealed at 603 K for 330 min. This value of T_{ai} is expected to provide a suggestion for the proper annealing temperature of other amorphous soft magnetic alloys.

Keywords: amorphous alloy; long-time annealing; soft magnetic properties; magnetic domain

Citation: Jia, J.; Wu, Y.; Shi, L.; Wang, R.; Guo, W.; Bu, H.; Shao, Y.; Chen, N.; Yao, K. Influence of Annealing Process on Soft Magnetic Properties of Fe-B-C-Si-P Amorphous Alloys. *Materials* **2024**, *17*, 1447. https://doi.org/10.3390/ma17061447

Academic Editors: Francesco Baino and Maziar Montazerian

Received: 18 February 2024
Revised: 9 March 2024
Accepted: 11 March 2024
Published: 21 March 2024

1. Introduction

Among the diverse soft magnetic materials, Fe-based amorphous alloys have attracted intensive attention due to their highly comprehensive soft magnetic performance, including low coercivity (H_c) and core loss (W) [1–4]. The structure of Fe-based amorphous alloys obtained through rapid solidification has various inhomogeneities, such as loose and dense atomic packing regions, regions with different internal stresses, and magnetic heterogeneous regions [5]. The H_c of Fe-based amorphous alloys is directly related to the inhomogeneity, internal stress, and free volume of amorphous alloys [5–8]. In order to reduce H_c and improve the soft magnetic properties, annealing is generally carried out near or above the Curie temperature (T_C) of amorphous alloys [5,9]. Above T_C, amorphous alloys are paramagnetic, so the stress release and structural relaxation are no longer affected by the local internal magnetic field [5,9,10]. Therefore, the magnetic domain structure is optimized, thus greatly improving the soft magnetic properties.

At present, the annealing time of amorphous alloys reported in the literature is relatively short, especially for those with a relatively high iron content; most of them are no more than 30 min [9,11–15]. However, for the industrial production of amorphous alloy products, long-time annealing is of great importance. Due to the characteristics of the furnace structure and the large volume of materials, the time required for uniform temperature distribution in the industrial production process is longer than that under experimental conditions. The time required to reach the set temperature for different locations in the furnace is different, but the properties of materials annealed in the same batch need to be as similar as possible. Therefore, it is required that the properties of amorphous alloys be kept stable during the annealing time for as long as possible.

A few studies have suggested that when annealing for a long time, even if the annealing temperature is slightly lower than T_C, good soft magnetic properties can also be obtained [16,17]. Thus, the question of how to determine the optimal annealing temperature for long-time annealing is important. T_C is a key temperature parameter used to describe the property transition of magnetic materials from ferromagnetic to paramagnetic; it is often used as a criterion for selecting the optimal annealing temperature in short-time annealing. Similarly, it is important to find a way to determine the optimal annealing temperature in long-time annealing and to understand the variation in magnetic properties with temperature.

In this study, $Fe_{81.4}B_{13.2}C_{2.8}Si_{1.8}P_{0.8}$ and $Fe_{82.2}B_{12.4}C_{2.8}Si_{1.8}P_{0.8}$ amorphous alloys with relatively high Fe content were designed and prepared. The effects of the annealing temperature and time on the soft magnetic properties, magnetic domain structure, and magnetization process of the amorphous alloys were systematically studied. The correlation between the magnetic properties and the structure of the annealed amorphous alloys is discussed, and the process for the magnetic property adjustment of Fe-based amorphous alloys in long-time annealing is investigated.

2. Materials and Methods

Amorphous alloy ribbons with nominal compositions of $Fe_{81.4}B_{13.2}C_{2.8}Si_{1.8}P_{0.8}$ (denoted as $Fe_{81.4}$) and $Fe_{82.2}B_{12.4}C_{2.8}Si_{1.8}P_{0.8}$ (denoted as $Fe_{82.2}$) were produced with single-roller spinning. The thermal properties of the amorphous alloys were examined using differential scanning calorimetry (DSC, Netzsch STA 449 F3, Netzsch, Selb, Germany) at a heating rate of 40 K/min. The temperature dependence of magnetization of the amorphous alloys was measured using superconducting quantum interference device (SQUID, MPMS-3, Quantum Design, San Diego, CA, USA) magnetometry under an applied field of 800 kA/m at a heating rate of 10 K/min. The ribbons, with a width of about 1 mm and a thickness of about 25 μm, were cut to an 80 mm length for subsequent annealing and measurements. The structures of the as-spun and annealed samples were identified using X-ray diffraction (XRD, Rigaku D/max 2500, Rigaku, Tokyo, Japan) with Cu Kα radiation. The structure of the as-spun $Fe_{82.2}$ amorphous alloy ribbon was also identified using high-resolution transmission electron microscopy (HRTEM, FEI Tecnai G2 F20, FEI, Hillsboro, OR, USA). The static magnetization curves and hysteresis loops were measured using a DC B-H hysteresis loop tracer (Linkjoin MATS-2010SD, Linkjoin, Loudi, China) under a field of 800 A/m. The domain structures were observed with a magneto-optical Kerr microscope (MOKE, Zeiss Imager D2m, Zeiss, Oberkochen, Germany).

In order to explore the effect of the annealing process on the soft magnetic properties of amorphous alloys, isothermal annealing treatments of the amorphous ribbons were carried out with the normal annealing (NA) process. This consisted of the following three steps: (1) the ribbon sample was fixed in a copper holder and then sealed in a quartz tube filled with argon gas; (2) the temperature inside the electric tube furnace was raised to the set value, and the quartz tube was pushed into the furnace; (3) after holding in the furnace for a given time, the quartz tube was pulled out of the furnace and quenched in water to room temperature.

3. Results and Discussion

In order to enhance the saturation magnetic flux density (B_s) of Fe-based amorphous alloys, the Fe content should be increased in the alloys. Based on former research results and considering the synergetic effect of metalloid elements B, C, Si, and P [17–21], two alloys with nominal compositions of $Fe_{81.4}B_{13.2}C_{2.8}Si_{1.8}P_{0.8}$ and $Fe_{82.2}B_{12.4}C_{2.8}Si_{1.8}P_{0.8}$ were designed and prepared via single-roller spinning. The structure of the prepared alloy ribbons was examined using the XRD method. As shown in Figure 1, no sharp diffraction peak corresponding to the crystalline phases in the XRD patterns of the as-spun $Fe_{81.4}$ and $Fe_{82.2}$ ribbons (black lines in Figure 1a and 1b, respectively) can be observed, indicating that both of them possessed an amorphous structure. The HRTEM image and SAED pattern in Figure 2 further confirm the amorphous nature of the as-spun $Fe_{82.2}$ ribbon. This implies that the designed alloys possessed good glass-forming abilities. The thermal properties of the as-spun ribbons, including the Curie temperature (T_C) and the onset temperature of crystallization (T_x), were determined from the DSC curves shown in Figure 3. The T_C and T_x of the $Fe_{81.4}$ amorphous ribbons were 661 K and 776 K, respectively, and those of $Fe_{82.2}$ were 635 K and 766 K, respectively. This indicates that the value of $T_x - T_C$ was over 110 K. When the Fe content was slightly increased by 0.8 at.% (the B content was reduced by 0.8 at.%), the T_C and T_x of the Fe-based amorphous alloy were clearly reduced. The decrease in the T_x is due to the decrease in thermal stability caused by the increase in Fe content and the decrease in B content [22,23]. Meanwhile, the decrease in T_C is due to the decrease in the exchange interaction [18,24].

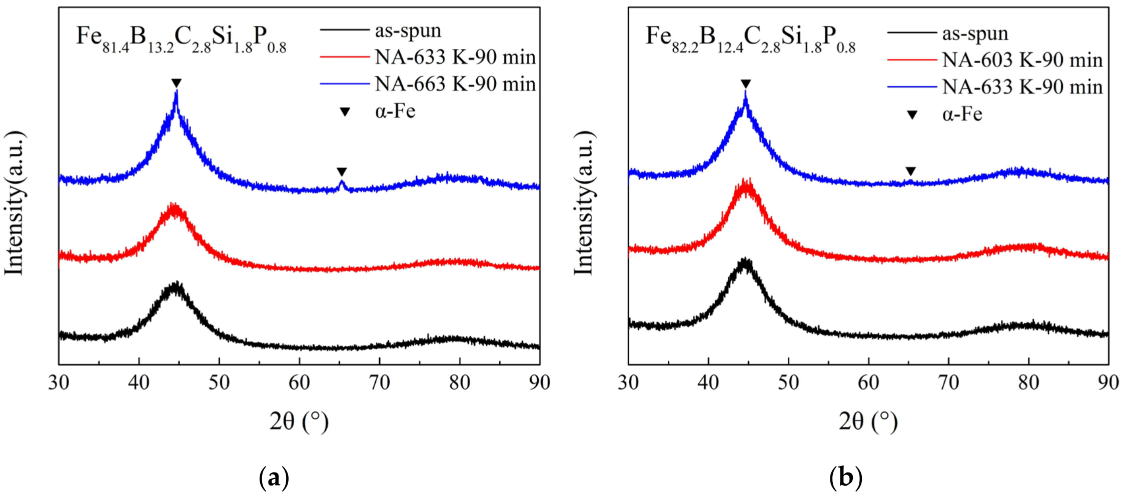

Figure 1. Smooth-side XRD patterns of as-spun ribbons and ribbons with different annealing temperatures for (**a**) $Fe_{81.4}B_{13.2}C_{2.8}Si_{1.8}P_{0.8}$ and (**b**) $Fe_{82.2}B_{12.4}C_{2.8}Si_{1.8}P_{0.8}$ amorphous alloys.

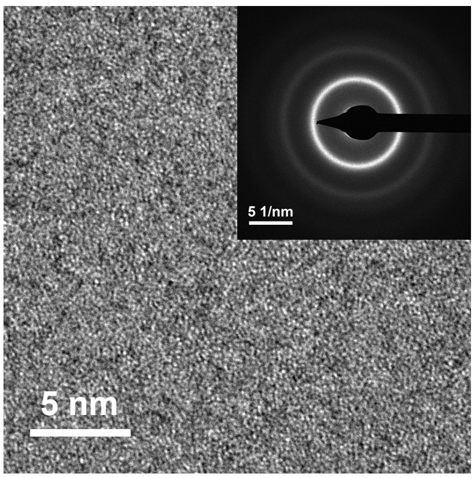

Figure 2. High-resolution transmission electron microscope (HRTEM) image and selected-area electron diffraction (SAED) pattern of $Fe_{82.2}B_{12.4}C_{2.8}Si_{1.8}P_{0.8}$ amorphous alloy.

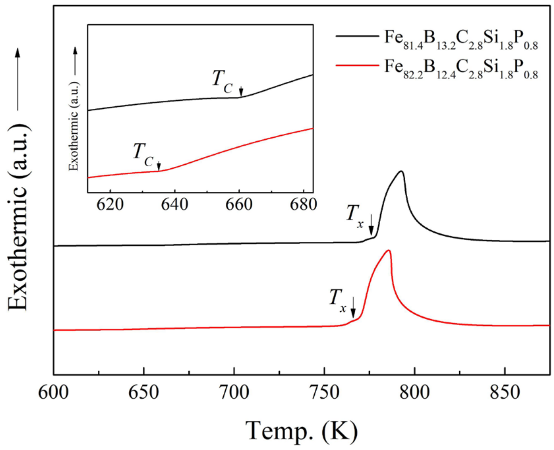

Figure 3. DSC curves of $Fe_{81.4}B_{13.2}C_{2.8}Si_{1.8}P_{0.8}$ and $Fe_{82.2}B_{12.4}C_{2.8}Si_{1.8}P_{0.8}$ amorphous alloys at a heating rate of 0.67 K/s. The inset shows an enlarged section of the curves around the Curie temperature T_C.

The amorphous ribbons were annealed at different temperatures from 563 K to 663 K with an interval of 10 K. Figure 4 shows the annealing temperature dependence of coercivity (H_c) and the magnetic flux density measured at an applied magnetic field of 800 A/m (B_{800}) for the $Fe_{81.4}B_{13.2}C_{2.8}Si_{1.8}P_{0.8}$ and $Fe_{82.2}B_{12.4}C_{2.8}Si_{1.8}P_{0.8}$ amorphous alloy ribbons after normal annealing for 90 min. With the increase in the annealing temperature, the H_c decreased to a low point at first, then maintained a stable state and finally increased rapidly. The stable region with the lowest H_c obtained in the experiment is defined as the optimal annealing temperature range. The lowest temperature of the optimum annealing temperature range is denoted as T_{a0}, and the highest temperature is denoted as T_{am}. The T_{a0} and T_{am} of the $Fe_{81.4}$ amorphous alloy were 623 K and 653 K, respectively, while the T_{a0} and T_{am} of the $Fe_{82.2}$ amorphous alloy were 593 K and 623 K, respectively. As the annealing temperature increased, the B_{800} of the alloys initially increased then reached a plateau and finally declined. B_{800} is a comprehensive reflection of the B_s, H_c, and permeability [25]. The initial temperatures of the B_{800} plateau were 613 K and 573 K for $Fe_{81.4}$ and $Fe_{82.2}$, respectively, which are lower than T_{a0}. However, the end temperature of the B_{800} plateau was equal to T_{am}. The reduction in H_c was due to the relaxation of stress and the reduction in the free volume [6]. However, spontaneous magnetization can affect the relaxation progress of amorphous alloys [5]. Therefore, the beginning of the optimum annealing temperature range of H_c did not coincide with the starting temperature of relaxation. The present results show that both the $Fe_{81.4}$ and $Fe_{82.2}$ amorphous alloys exhibited an optimized annealing temperature range of 30 K, together with B_{800} and H_c values of 1.64–1.65 T and 2.0–2.5 A/m and 1.65–1.66 T and 1.3–2.7 A/m, respectively. This indicates that, after annealing, the developed amorphous alloys were excellent soft magnetic materials, exhibiting a high B_{800} and low H_c (Figure 4).

In order to understand the effect of elements on the magnetic property, the temperature dependence of the saturation flux density (B_s) for the $Fe_{81.4}$ and $Fe_{82.2}$ amorphous alloys was obtained and studied (Figure 5). At a temperature of 5 K, the B_s values of the $Fe_{81.4}$ and $Fe_{82.2}$ amorphous alloys were 1.84 T and 1.92 T, respectively. At a temperature of 5 K, the B_s values of the $Fe_{81.4}$ and $Fe_{82.2}$ amorphous alloys were 1.84 T and 1.92 T, respectively. When the Fe content increased, the proportion of ferromagnetic atoms increased; thus, the total magnetic moment increased, leading to an increase in the B_s near 0 K [18,26]. As the temperature increased, the atomic thermal motion increased. In ferromagnetic materials, the thermal motion of atoms disturbs the spontaneous magnetization of atomic magnetic moments [24]. As a result, the B_s of the $Fe_{81.4}$ and $Fe_{82.2}$ amorphous alloys decreased continuously with the increase in temperature, until it reached the lowest point. The temperature with the lowest B_s is denoted as T_{x0}. When the temperature exceeded T_{x0}, the B_s began to increase, which was caused by crystallization of the amorphous alloys. Finally, the B_s decreased again because the spontaneous magnetization of α-Fe decreased rapidly. In a sense, T_{x0} is the temperature at which crystallization is observed on the $B_s(T)$–T curve to have a noticeable effect on the magnetic properties.

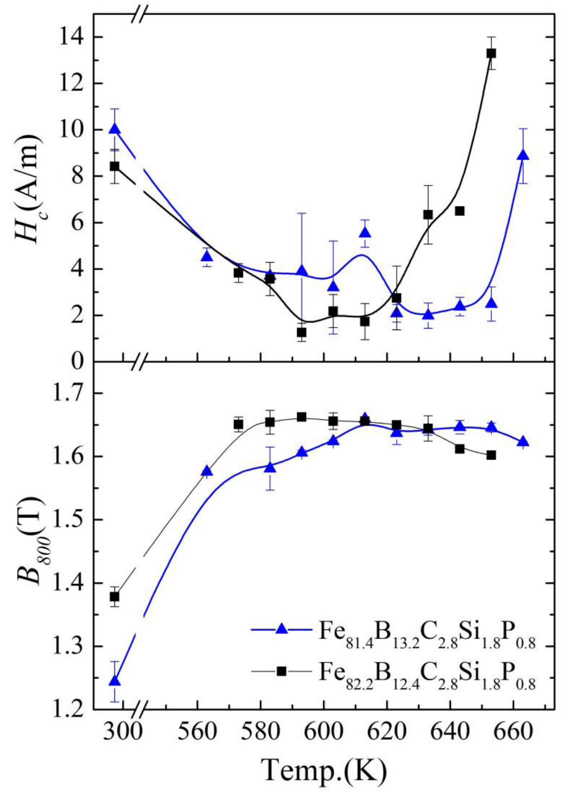

Figure 4. Annealing temperature dependence of H_c (coercivity) and B_{800} for the $Fe_{81.4}B_{13.2}C_{2.8}Si_{1.8}P_{0.8}$ and $Fe_{82.2}B_{12.4}C_{2.8}Si_{1.8}P_{0.8}$ amorphous alloy ribbons after normal annealing for 90 min.

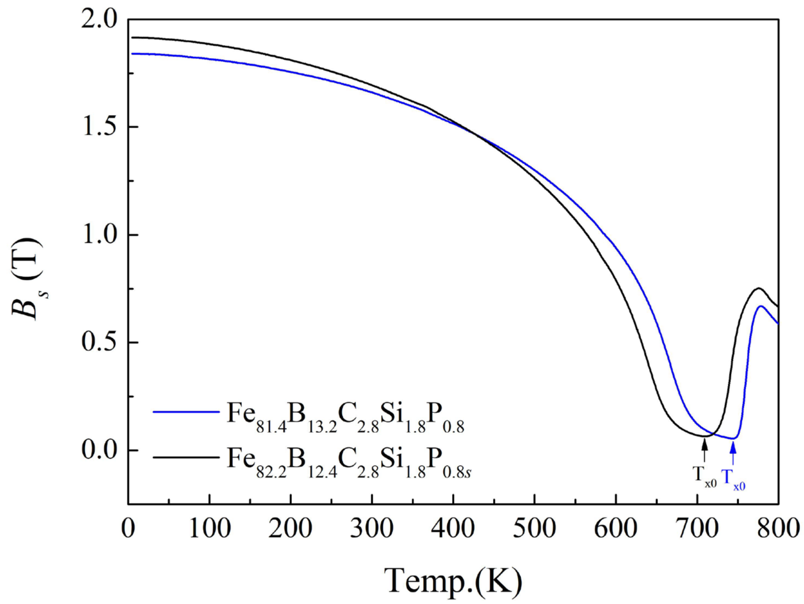

Figure 5. Temperature dependence of B_s for $Fe_{81.4}B_{13.2}C_{2.8}Si_{1.8}P_{0.8}$ and $Fe_{82.2}B_{12.4}C_{2.8}Si_{1.8}P_{0.8}$ amorphous alloys.

The shape of the $B_s(T)$–T curve is related to the strength of the exchange interaction [18,24]. In order to visualize the declining rate of the B_s with increasing temperature, the reduced saturation flux density $B_s(T)/B_s(5\text{K})$ as a function of temperature (T) and the derived first derivative of B_s with respect to T are shown in Figure 6. For the $Fe_{81.4}$ and $Fe_{82.2}$ amorphous alloys, the $B_s(T)/B_s(5K)$–T and dB_s/dT–T curves are similar. At first, the $B_s(T)/B_s(5K)$ and dB_s/dT decreased slowly with the increase in temperature. When the temperature continued rising to near the temperature denoted as T_{ai}, at which $B_s(T)/B_s(5K)$ = 45%, the value of dB_s/dT began to decrease rapidly. Increasing the temperature further, dB_s/dT decreased further and reached the lowest level. The corresponding temperature is denoted as T_{C0} (as shown in Figure 6). When the temperature was higher than T_{C0} but lower than T_{x0}, dB_s/dT gradually increased with the increase in temperature. Meanwhile, the decrease in $B_s(T)/B_s(5K)$ developed slowly. In other words, T_{C0} represents the temperature at which the spontaneous magnetization of the alloy changed the most dramatically, i.e., the Curie temperature (the temperature at which ferromagnetism transforms into paramagnetism). The value of T_{C0} was indeed close to the Curie temperature obtained from the DSC curve (T_C), as shown in Table 1.

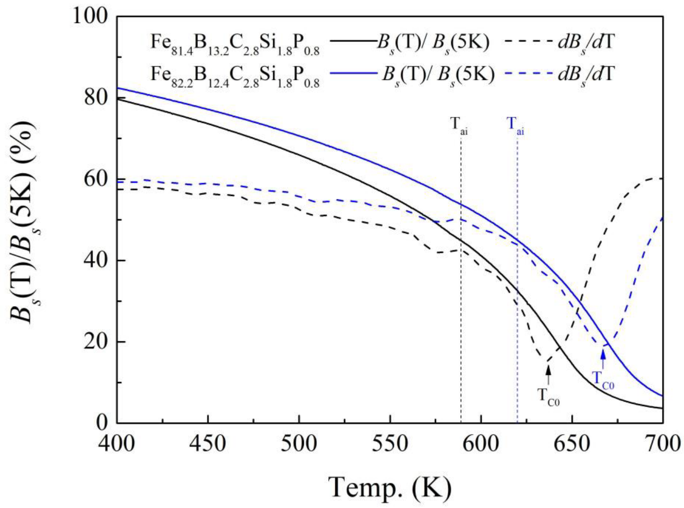

Figure 6. Reduced saturation flux density $B_s(T)/B_s(5K)$ as a function of temperature for $Fe_{81.4}B_{13.2}C_{2.8}Si_{1.8}P_{0.8}$ and $Fe_{82.2}B_{12.4}C_{2.8}Si_{1.8}P_{0.8}$ amorphous alloys. Note that the dotted lines are the first derivative of B_s with respect to temperature T for the alloys.

Table 1. Several temperature parameters mentioned in this article for $Fe_{81.4}B_{13.2}C_{2.8}Si_{1.8}P_{0.8}$ and $Fe_{82.2}B_{12.4}C_{2.8}Si_{1.8}P_{0.8}$ amorphous alloys.

Alloy	T_{a0} (K)	T_{am} (K)	T_{ai} (K)	T_{C0} (K)	T_{x0} (K)	T_C (K)	T_x (K)
$Fe_{81.4}B_{13.2}C_{2.8}Si_{1.8}P_{0.8}$	623	653	620	667	744	661	776
$Fe_{82.2}B_{12.4}C_{2.8}Si_{1.8}P_{0.8}$	593	623	589	637	709	635	766

T_{a0} and T_{am} are the lowest temperature and the highest temperature of the optimum annealing temperature range, as shown in Figure 4; T_{x0}, T_{ai}, and T_{C0} are the characteristic temperatures, as shown in Figures 5 and 6; T_C and T_x are the Curie temperature and the onset temperature of crystallization, determined from the DSC curves shown in Figure 3.

Although the $B_s(T)$–T, $B_s(T)/B_s(5K)$–T, and dB_s/dT–T curves of the $Fe_{81.4}$ and $Fe_{82.2}$ amorphous alloys are similar, the T_{ai} and T_{C0} of the $Fe_{82.2}$ amorphous alloy were lower than those of the $Fe_{81.4}$ amorphous alloy. This is due to the difference in the strength of the exchange interaction for the $Fe_{81.4}$ and $Fe_{82.2}$ amorphous alloys. The metalloid content of the $Fe_{82.2}$ amorphous alloy was lower than that of the $Fe_{81.4}$ amorphous alloy. The decrease in the metalloid content causes a reduction of the interatomic distance between the Fe atoms [18,24]. According to the Bethe–Slater curve [24], the strength of the exchange interaction will decrease with the decrease in the interatomic distances between Fe atoms. Therefore, the dB_s/dT increases, resulting in a decrease in T_{ai} and T_{C0}.

By examining and analyzing the results shown in Figures 4–6, it is not difficult to find that T_{a0} is approximate to T_{ai}. This may have been caused by the effect of spontaneous magnetization on the alloy relaxation process of these amorphous alloys. When the annealing temperature is lower than T_{ai} but sufficient to allow short-distance movement of the atoms, the thermal motion of the atoms may cause changes in the local structure. On the one hand, long-term heat treatment at this temperature is enough to eliminate the influence of stress on H_c, so that H_c can be reduced compared to the cast state. On the other hand, the spontaneous magnetization is still high. Spontaneous magnetization will strengthen the local magnetic anisotropy [5,9,27], so it is difficult to achieve the optimal low coercivity after annealing. When the annealing temperature is higher than T_{ai}, the decline in the dB_s/dT value begins to accelerate, and the $B_s(T)$ decreases to less than half of the B_s near 0 K ($B_s(T)/B_s(5K) \leq 45\%$), which demonstrates that the ferromagnetism of amorphous alloys is greatly weakened. The effect of the inner magnetic field generated by spontaneous magnetization on the relaxation behavior becomes negligible. The magnetic anisotropy of the alloy is reduced, and the soft magnetic properties are greatly improved. Based on the above analysis, we provide a simple way to determine the lowest temperature T_{ai} ($B_s(T_{ai})/B_s(5K) = 45\%$) of the optimum annealing temperature range for the Fe-based amorphous alloys with a relatively low Curie temperature, similar to the current amorphous alloys.

The magnetic domain structures of the amorphous alloy samples that experienced different annealing processes were characterized using a magneto-optical Kerr microscope, and the effect of spontaneous magnetization on the soft magnetic properties is discussed. Figure 7 shows the domain structures of the as-spun, NA-633 K-annealed and NA-603 K-annealed $Fe_{81.4}B_{13.2}C_{2.8}Si_{1.8}P_{0.8}$ amorphous alloy samples in the demagnetized state. There were two types of typical domains in the as-spun $Fe_{81.4}$ amorphous alloy sample (Figure 7a): wide-curved domains and narrow fingerprint domains. These are caused by tensile stress and compressive stress [5,28,29]. After normal annealing at 633 K, the domains of the sample appeared as a broad strip pattern oriented slightly away from the length direction of the amorphous ribbon, demonstrating a low domain energy, homogenous structure, and low stress state [30]. In contrast, more domain branches and rugged edges were present in the magnetic domain structure of the NA-603 K $Fe_{81.4}$ amorphous alloy sample, and their direction deviated from the length direction, indicating a strong pinning effect. This phenomenon can be attributed to the magnetic anisotropy induced by spontaneous magnetization during the annealing process, because the annealing temperature was lower than T_{ai} [5,9,27]. This shows that the annealing temperature above T_{ai} is important for removing the pinning effect to obtain a low H_c, as shown in Figure 4.

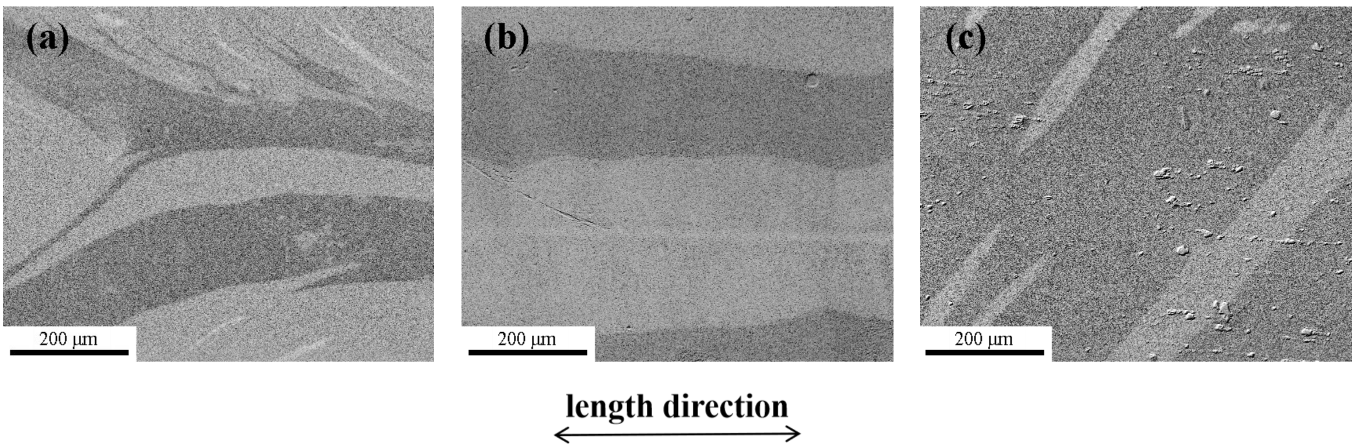

Figure 7. Magnetic domains in the demagnetized state for $Fe_{81.4}B_{13.2}C_{2.8}Si_{1.8}P_{0.8}$ amorphous alloy samples: (**a**) as-spun, (**b**) NA-633 K, and (**c**) NA-603 K.

It is well known that amorphous alloys are of a thermodynamic metastable state. They will eventually crystallize as long as the annealing time is long enough at a high enough temperature. Moreover, the higher the annealing temperature is, the shorter the time required for crystallization. Therefore, the T_{am} is actually also related to the annealing time.

When the annealing time is 90 min, crystallization of the $Fe_{82.2}$ amorphous alloy occurs at 633 K, resulting in the H_c increasing to 6.3 A/m. However, after annealing at 633 K for 60 min, the H_c of the amorphous alloy is 1.4 A/m; that is, the highest temperature of the optimum annealing temperature range for 60 min is not lower than 633 K.

Figure 8 illustrates the annealing time dependence of H_c and B_{800} for the $Fe_{82.2}B_{12.4}C_{2.8}Si_{1.8}P_{0.8}$ amorphous alloy ribbons with normal annealing at different temperatures. Three different annealing temperatures were selected for the $Fe_{82.2}$ amorphous alloy: T_{a1} = 603 K, T_{a2} = T_{am} (90 min) = 623 K, and T_{a3} = 633 K, respectively. Overall, with the increase in the annealing time, the B_{800} of the alloys increased initially and then remained relatively stable. When T_{a3} = 633 K, the H_c first decreased rapidly as the annealing time increased, then remained stable for a short time (30–60 min), and rose quickly after the annealing time reached 90 min. When T_{a2} = 623 K, the H_c showed a concave shape with respect to annealing time: the H_c first decreased rapidly, then decreased to 1.3 A/m after 30 min, and remained below 3 A/m within 30–120 min. Up to an annealing time of 150 min, the H_c rose to 4.6 A/m. However, when the annealing temperature decreased to T_{a1} (603 K), the coercivity H_c of the annealed samples exhibited very strong stability with the increase in annealing time. Even when the annealing time was extended to 330 min, the H_c was still only 1.9 A/m. For the $Fe_{82.2}$ amorphous alloy, T_{a1} was slightly higher than T_{ai} ($T_{a1} - T_{ai} < 15$ K).

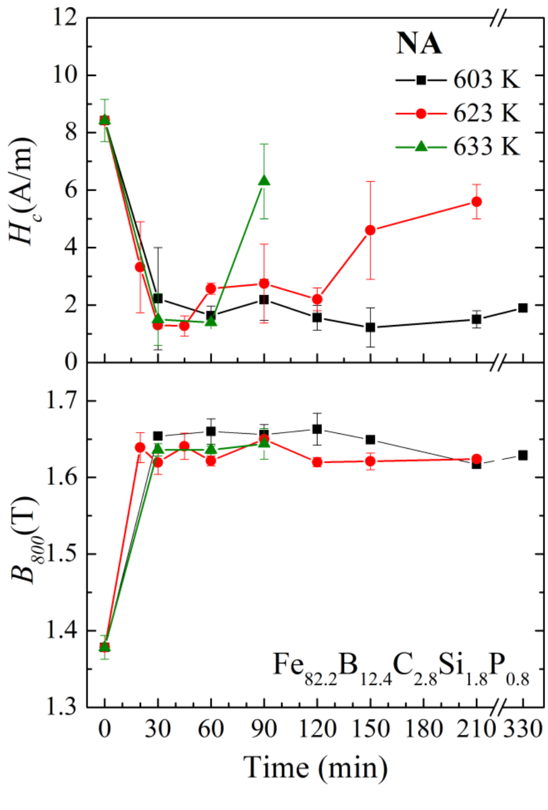

Figure 8. Annealing time dependence of H_c and B_{800} for the $Fe_{82.2}B_{12.4}C_{2.8}Si_{1.8}P_{0.8}$ amorphous alloy ribbons with normal annealing at different temperatures.

The annealing time dependence of H_c and B_{800} for the $Fe_{81.4}B_{13.2}C_{2.8}Si_{1.8}P_{0.8}$ amorphous alloy ribbons with normal annealing at different temperatures is shown in Figure 9. Two different annealing temperatures were selected for the $Fe_{81.4}$ amorphous alloy, which were T_{a4} = 633 K and T_{a5} = 663 K, respectively. For both annealing temperatures, with the increase in annealing time, the B_{800} increased rapidly at first and then became stable. When the annealing temperature was T_{a4} = 633 K, the H_c rapidly decreased to about 1 A/m and then slowly increased. The H_c remained at 2.7 A/m after 150 min of annealing. However, when the annealing temperature increased to T_{a5} = 663 K, the H_c remained relatively stable only within 30–60 min, and at this time, the H_c was 2.8–3.7 A/m, which was significantly higher than that at 633 K. Although the H_c of the $Fe_{81.4}$ amorphous alloy shown in Figure 9 is higher than that of the $Fe_{82.2}$ amorphous alloy shown in Figure 8, it can also be seen that when the annealing temperature is selected properly (slightly higher than T_{ai}), the soft magnetic properties can remain relatively stable for a longer period of time.

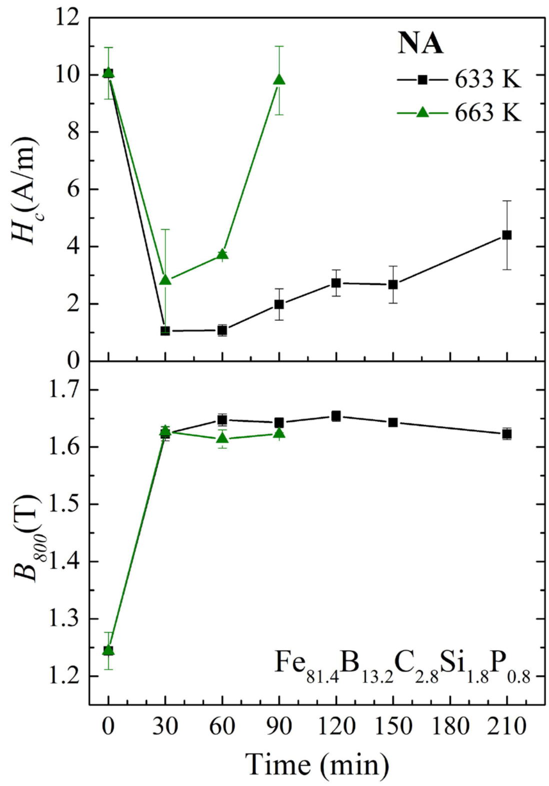

Figure 9. Annealing time dependence of H_c and B_{800} for the $Fe_{81.4}B_{13.2}C_{2.8}Si_{1.8}P_{0.8}$ amorphous alloy ribbons with normal annealing at different temperatures.

The increase in H_c in the long-term annealed samples shown in Figures 8 and 9 is also due to the formation of nanocrystalline clusters and the growth of these clusters. Figure 10 shows the smooth-side XRD patterns of the ribbons with different annealing times and temperatures for the $Fe_{81.4}$ and $Fe_{82.2}$ amorphous alloys. As shown in Figure 10, few weak diffraction peaks corresponding to the α-Fe crystalline phase can be detected in the smooth-side XRD patterns of the $Fe_{81.4}$ ribbons annealed at 633 K for 210 min and the $Fe_{82.2}$ ribbons annealed at 623 K for 150 min.

Figure 11 shows the magnetic domain structures of the as-spun, NA-623K-45 min-annealed and NA-623K-210 min annealed $Fe_{82.2}B_{12.4}C_{2.8}Si_{1.8}P_{0.8}$ amorphous alloy samples in the demagnetized state. Wide-curved domains and narrow fingerprint domains, caused by tensile stress and compressive stress [5,29], are observed in the as-spun $Fe_{82.2}$ amorphous alloy sample (Figure 11a). The domains of the sample annealing at 623 K for 45 min appear as a broad strip pattern oriented slightly away from the length direction of the amorphous ribbon, demonstrating the low domain energy, homogenous structure, and low stress state. However, for the sample annealed at 623K for 210 min, the magnetic domain structure with rugged edges can be clearly observed (Figure 11c), which is quite different from those in the NA-623 K-45 min annealed sample (Figure 11b). This indicates that a strong pinning effect exists, induced by partial crystallization resulting from long-term annealing (see Figure 10b) [5,9,27,32].

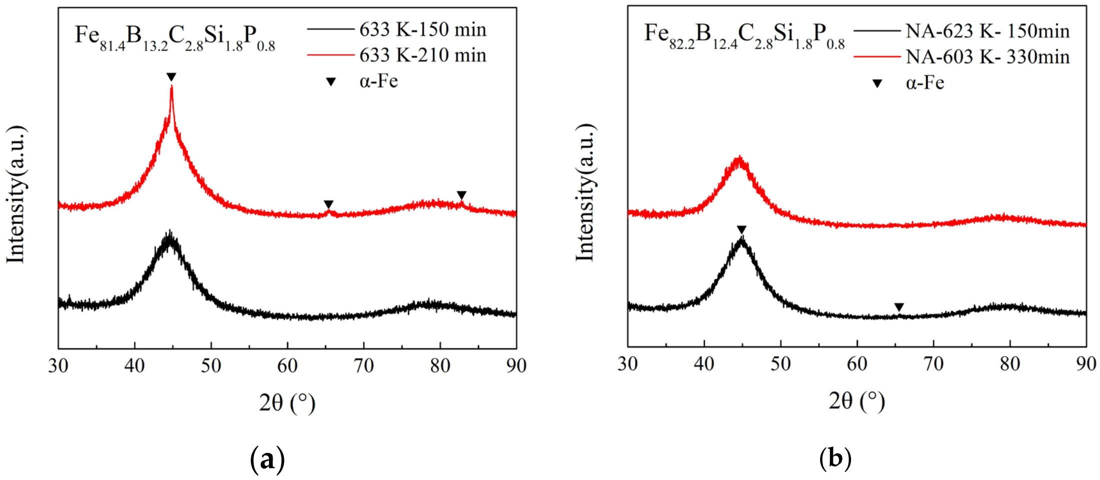

Figure 10. Smooth-side XRD patterns of ribbons with different annealing times and temperatures for (**a**) $Fe_{81.4}B_{13.2}C_{2.8}Si_{1.8}P_{0.8}$ and (**b**) $Fe_{82.2}B_{12.4}C_{2.8}Si_{1.8}P_{0.8}$ amorphous alloys.

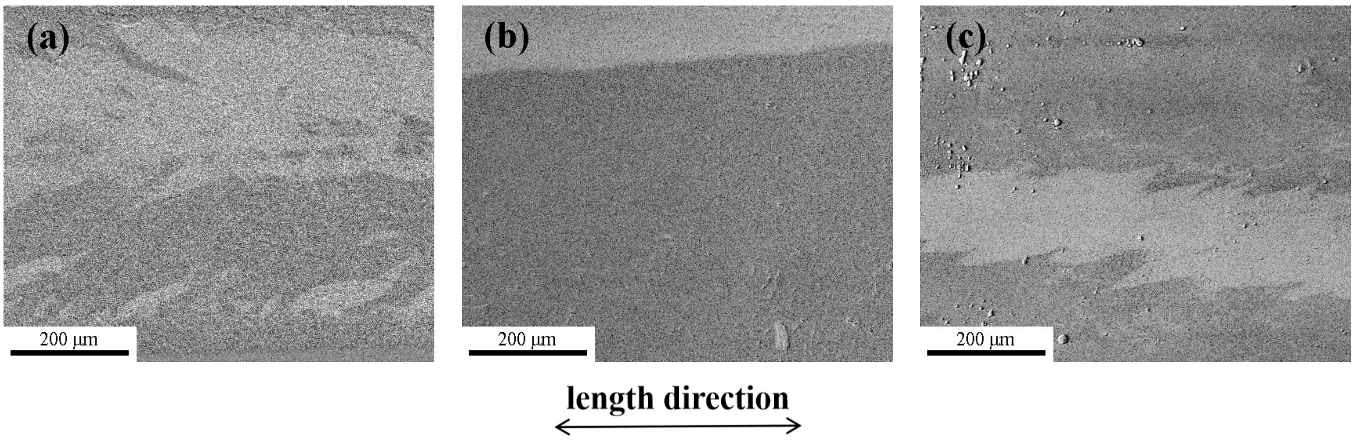

Figure 11. Magnetic domains in the demagnetized state for the $Fe_{82.2}B_{12.4}C_{2.8}Si_{1.8}P_{0.8}$ amorphous alloy samples: (**a**) as-spun, (**b**) NA-623K-45 min, and (**c**) NA-623K-210 min.

The above results indicate that when the annealing temperature is selected properly (slightly higher than T_{ai}), excellent and stable soft magnetic properties of amorphous alloys can be obtained through annealing even if the annealing is maintained for a very long time. Annealing slightly above T_{ai} could eliminate the influence of stress and the internal magnetic field on the H_c. In addition, a relatively low annealing temperature could reduce the possibility of crystallization. This result is of great significance for designing an annealing process for industrial applications.

4. Conclusions

The effects of annealing process parameters, including the annealing temperature and time, on the soft magnetic properties and magnetic domain structures of $Fe_{81.4}B_{13.2}C_{2.8}Si_{1.8}P_{0.8}$ and $Fe_{82.2}B_{12.4}C_{2.8}Si_{1.8}P_{0.8}$ amorphous alloys were systematically investigated, and the conclusions are summarized as follows:

(1) $Fe_{81.4}B_{13.2}C_{2.8}Si_{1.8}P_{0.8}$ and $Fe_{82.2}B_{12.4}C_{2.8}Si_{1.8}P_{0.8}$ amorphous alloys were designed and prepared. This revealed that a lowest and highest temperature, denoted as T_{a0} and T_{am}, respectively, exists for the optimum annealing of the amorphous alloys. The H_c of the $Fe_{81.4}$ and $Fe_{82.2}$ amorphous alloys annealed at T_{a0}–T_{am} for 90 min was 1.3–2.7 A/m, together with the B_{800} of 1.64–1.66 T. T_{a0} is determined by the variation in the magnetic properties with temperature. T_{am} is the temperature related to the crystallization of amorphous alloys.

(2) It was found that on the $B_s(T)$–T curve, there is a temperature T_{ai} at which the dB_s/dT begins to decrease rapidly, and $B_s(T_{ai})/B_s(5\mathrm{K})$ = 45%. When the amorphous alloys were annealed slightly above T_{ai}, the effect of the inner magnetic field generated by spontaneous magnetization on the relaxation behavior became very weak. That is, the temperature T_{ai} could be employed as a characteristic temperature. Slightly above T_{ai}, an optimized annealing temperature T_{a0} for the Fe-based amorphous alloys with a relatively low Curie temperature, similar to the studied alloys, could be determined quickly.

(3) When the annealing temperature was selected properly (slightly higher than T_{ai}), the soft magnetic properties of amorphous alloys could remain excellent and stable even if annealed for a very long time. The H_c of the $Fe_{82.2}B_{12.4}C_{2.8}Si_{1.8}P_{0.8}$ amorphous alloy annealed at T_{a1} = 603 K was only 1.9 A/m, while the annealing time was extended to 330 min.

Author Contributions: Conceptualization, J.J. and K.Y.; investigation, J.J., Y.W. and R.W.; data curation, J.J., Y.W., R.W. and W.G.; formal analysis, J.J., Y.W., L.S., R.W., W.G., H.B., Y.S., N.C. and K.Y.; visualization, J.J.; writing—original draft, J.J.; writing—review and editing, J.J., K.Y. and L.S. All authors have read and agreed to the published version of the manuscript.

Funding: This research was funded by the National Key Basic Research and Development Program, grant numbers 2022YFB3804100 and 2022YFB4200800, and the National Natural Science Foundation of China, grant numbers 52271148 and 51871129.

Institutional Review Board Statement: Not applicable.

Informed Consent Statement: Not applicable.

Data Availability Statement: The raw data supporting the conclusions of this article will be made available by the authors upon request.

Conflicts of Interest: The authors declare no conflicts of interest.

References

1. Hasegawa, R. Application of amorphous magnetic alloys. *Mater. Sci. Eng. A* **2004**, *375*, 90–97. [CrossRef]
2. Herzer, G. Modern soft magnets: Amorphous and nanocrystalline materials. *Acta Mater.* **2013**, *61*, 718–734. [CrossRef]
3. Milanez, D.H.; Faria, L.I.L.; Leiva, D.R.; Kiminami, C.S.; Botta, W.J. Assessing technological developments in amorphous/glassy metallic alloys using patent indicators. *J. Alloys Compd.* **2017**, *716*, 330–335. [CrossRef]
4. Silveyra, J.M.; Ferrara, E.; Huber, D.L.; Monson, T.C. Soft magnetic materials for a sustainable and electrified world. *Science* **2018**, *362*, 418–426. [CrossRef] [PubMed]
5. Zhao, C.L.; Wang, A.D.; Yue, S.Q.; Liu, T.; He, A.N.; Chang, C.T.; Wang, X.M.; Liu, C.T. Significant improvement of soft magnetic properties for Fe(Co) BPSiC amorphous alloys by magnetic field annealing. *J. Alloys Compd.* **2018**, *742*, 220–225. [CrossRef]
6. Kronmuller, H. Micromagnetism and Microstructure of Amorphous-Alloys. *J. Appl. Phys.* **1981**, *52*, 1859–1864. [CrossRef]
7. Kronmuller, H.; Groger, B. Domains, Domain-Walls and the Coercive Field of Amorphous Ferromagnets. *J. Phys.* **1981**, *42*, 1285–1292. [CrossRef]
8. Li, Z.; Yao, K.F.; Liu, T.C.; Li, X.; Wang, S. Effect of Annealing on the Magnetic Properties of FeCoNiCuNbSiB Soft Magnetic Alloys. *Front. Mater.* **2022**, *8*, 805609. [CrossRef]
9. Li, H.; He, A.N.; Wang, A.D.; Xie, L.; Li, Q.; Zhao, C.L.; Zhang, G.Y.; Chen, P.B. Improvement of soft magnetic properties for distinctly high Fe content amorphous alloys via longitudinal magnetic field annealing. *J. Magn. Magn. Mater.* **2019**, *471*, 110–115. [CrossRef]
10. Tejedor, M.; García, J.A.; Carrizo, J.; Elbaile, L.; Santos, J.D. Stress relief and magnetic properties of magnetostrictive $Fe_{79}B_{16}Si_5$ amorphous magnetic ribbons. *J. Magn. Magn. Mater.* **1999**, *202*, 485–491. [CrossRef]
11. Makino, A.; Kubota, T.; Chang, C.; Makabe, M.; Inoue, A. FeSiBP bulk metallic glasses with high magnetization and excellent magnetic softness. *J. Magn. Magn. Mater.* **2008**, *320*, 2499–2503. [CrossRef]
12. Liang, X.F.; He, A.N.; Wang, A.D.; Pang, J.; Wang, C.J.; Chang, C.T.; Qiu, K.Q.; Wang, X.M.; Liu, C.T. Fe content dependence of magnetic properties and bending ductility of FeSiBPC amorphous alloy ribbons. *J. Alloys Compd.* **2017**, *694*, 1260–1264. [CrossRef]
13. Yue, S.; Zhang, H.; Cheng, R.; Wang, A.; Dong, Y.; He, A.; Ni, H.; Liu, C.-T. Magnetic and thermal stabilities of FeSiB eutectic amorphous alloys: Compositional effects. *J. Alloys Compd.* **2019**, *776*, 833–838. [CrossRef]
14. Zhang, G.; Zhang, H.; Yue, S.; Wang, A.; He, A.; Cheng, R.; Dong, Y.; Ni, H.; Liu, C.-T. Ultra-low cost and energy-efficient production of FePCSi amorphous alloys with pretreated molten iron from a blast furnace. *J. Non-Cryst. Solids* **2019**, *514*, 108–115. [CrossRef]

15. Tokmakova, E.N.; Vvedenskiy, V.Y. Effect of annealing in unsaturated magnetic field on the magnetic properties of an amorphous alloy $Fe_{77}Ni_1Si_9B_{13}$. *J. Mater. Sci. Mater. Electron.* **2023**, *34*, 10. [CrossRef]
16. Hatta, S.; Egami, T.; Graham, C.D. Amorphous Alloys with Improved Room-Temperature Saturation Induction. *IEEE Trans. Magn.* **1978**, *14*, 1013–1015. [CrossRef]
17. Wang, A.D.; Zhao, C.L.; Men, H.; He, A.N.; Chang, C.T.; Wang, X.M.; Li, R.W. Fe-based amorphous alloys for wide ribbon production with high B-s and outstanding amorphous forming ability. *J. Alloys Compd.* **2015**, *630*, 209–213. [CrossRef]
18. Shi, L.X.; Hu, X.Y.; Li, Y.H.; Yuan, G.T.; Yao, K.F. The complementary effects of Fe and metalloids on the saturation magnetization of Fe-based amorphous alloys. *Intermetallics* **2021**, *131*, 107116. [CrossRef]
19. Mitera, M.; Naka, M.; Masumoto, T.; Kazama, N.; Watanabe, K. Effects of Metalloids on Magnetic-Properties of Iron Based Amorphous Alloys. *Phys. Status Solidi A* **1978**, *49*, K163–K166. [CrossRef]
20. Shi, L.X.; Yao, K.F. Composition design for Fe-based soft magnetic amorphous and nanocrystalline alloys with high Fe content. *Mater. Des.* **2020**, *189*, 108511. [CrossRef]
21. Liu, F.J.; Yao, K.F.; Ding, H.Y. Fe-based glassy alloys with high iron content and high saturation magnetization. *Intermetallics* **2011**, *19*, 1674–1677. [CrossRef]
22. Torrens-Serra, J.; Bruna, P.; Rodriguez-Viejo, J.; Roth, S.; Clavaguera-Mora, M.T. Effect of minor additions on the glass forming ability and magnetic properties of Fe-Nb-B based metallic glasses. *Intermetallics* **2010**, *18*, 773–780. [CrossRef]
23. Lashgari, H.R.; Chu, D.; Xie, S.S.; Sun, H.D.; Ferry, M.; Li, S. Composition dependence of the microstructure and soft magnetic properties of Fe-based amorphous/nanocrystalline alloys: A review study. *J. Non-Cryst. Solids* **2014**, *391*, 61–82. [CrossRef]
24. Cullity, B.D.; Graham, C.D. *Introduction to Magnetic Materials*, 2nd ed.; IEEE/Wiley: Hoboken, NJ, USA, 2009; pp. 115–149.
25. Shi, L.X.; Qin, X.L.; Yao, K.F. Tailoring soft magnetic properties of Fe-based amorphous alloys through C addition. *Prog. Nat. Sci. Mater. Int.* **2020**, *30*, 208–212. [CrossRef]
26. Graham, C.D.; Egami, T. Magnetic-properties of Amorphous Ribbon. *IEEE Trans. Magn.* **1979**, *15*, 1398–1403. [CrossRef]
27. Suzuki, K.; Herzer, G. Magnetic-field-induced anisotropies and exchange softening in Fe-rich nanocrystalline soft magnetic alloys. *Scr. Mater.* **2012**, *67*, 548–553. [CrossRef]
28. Obi, Y. The Stress Effect on Magnetic Domain Structure of Fe-Co Amorphous Alloys. *Appl. Phys.* **1979**, *18*, 119–121. [CrossRef]
29. Liu, J.P. *Nanoscale Magnetic Materials and Applications*; Springer: New York, NY, USA, 2009; pp. 275–304.
30. Azuma, D.; Hasegawa, R.; Saito, S.; Takahashi, M. Effect of residual strain in Fe-based amorphous alloys on field induced magnetic anisotropy and domain structure. *J. Appl. Phys.* **2013**, *113*, 17A339. [CrossRef]
31. Bayri, N.; Kolat, V.S.; Atalay, F.E.; Atalay, S. The effect of furnace annealing and surface crystallization on the anisotropy, ΔE and magnetoimpedance effects in FeCrSiB amorphous wires. *J. Phys. D Appl. Phys.* **2004**, *37*, 3067–3072. [CrossRef]
32. Fecova, L.; Richter, K.; Varga, R. Annealing Effect on Domain Wall Dynamics in Wires with Induced Gradient of Perpendicular Anisotropy. *IEEE Trans. Magn.* **2022**, *58*, 4301405. [CrossRef]
33. Lopatina, E.; Soldatov, I.; Budinsky, V.; Marsilius, M.; Schultz, L.; Herzer, G.; Schäfer, R. Surface crystallization and magnetic properties of $Fe_{84.3}Cu_{0.7}Si_4B_8P_3$ soft magnetic ribbons. *Acta Mater.* **2015**, *96*, 10–17. [CrossRef]